Advances in Concrete Construction, *Vol. 3, No. 4 (2015) 295-316*
DOI: http://dx.doi.org/10.12989/acc.2015.3.4.295

Bridge widening with composite steel-concrete girders: application and analysis of live load distribution

Yue Yang[1], Xiaoguang Zhang[1], Jiansheng Fan[*1] and Yu Bai[2]

[1]Department of Civil Engineering, Tsinghua University, Beijing, 100084, China
[2]Department of Civil Engineering, Monash University, Clayton, VIC 3800, Australia

(Received July 3, 2015, Revised January 25, 2016, Accepted January 29, 2016)

Abstract. A bridge widening technology using steel-concrete composite system was developed and is presented in this paper. The widened superstructure system consists of a newly built composite steel-concrete girder with concrete deck and steel diaphragms attached to the existing concrete girders. This method has been applied in several bridge widening projects in China, and one of those projects is presented in detail. Due to the higher stiffness-to-weight ratio and the rapid erection of composite girders, this widening method reveals benefits in both mechanical performance and construction. As only a few methods for the design of bridges with different types of girders are recommended in current design codes, a more accurate analytical method of estimating live load distribution on girder bridges was developed. In the analytical model, the effects of span length, girder pacing, diaphragms, concrete decks were considered, as well as the torsional and flexural stiffness of both composite box girders and concrete T girders. The study shows that the AASHTO LRFD specification procedures and the analytical models proposed in this paper closely approximate the live load distribution factors determined by finite element analysis. A parametric study was also conducted using the finite element method to evaluate the potential load carrying capacities of the existing concrete girders after widening.

Keywords: bridge widening; composite girder; distribution factor; field test; finite element analysis

1. Introduction

With the steady and rapid increase in the vehicle population in developing countries, many existing roadways are becoming inadequate for current or predicted traffic. Improvement of the road traffic capacity requires modernization of both roads and the bridges located along them. In many cases, the bridges, which cause bottlenecks in the road networks, are critical for improvement of traffic systems. Bridge engineers have two options for road modernization: replacing old bridges with new ones or widening existing bridges. For reasons of economy and minimization of traffic disruption during construction, bridge widening is commonly used.

Recent years, many researchers focused on the mechanical behavior of different bridge widening methods. Wang *et al*. (2011) proposed a new box girder widening method: SCWCGM, and conducted full-scale model test. Hong and Park (2014) conducted series of experiments to

∗Corresponding author, Professor, E-mail: fanjsh@tsinghua.edu.cn

http://www.techno-press.org/?journal=acc&subpage=7 ISSN: 2234-0912 (Print), 2234-179X (Online)

inspect concrete strength during bridge widening. Generally, selection of the widening technique for any bridge depends the type and material of the superstructure, the required dimensions after widening, the condition of the existing structures, and traffic requirements during construction. However, in some cases, the geometry and the condition of the existing bridge superstructure and substructure are insufficient to sustain the widened decks and the increased live load, in which case a different type of girder may be required for the widened portion of the bridge, e.g., composite steel-concrete girders for widening a concrete bridge. Given the higher stiffness and strength and lower self-weight of composite girders, benefits in both mechanical performance and economy can be provided in many instances. Besides, composite steel-concrete girder has better long-term effect than concrete box girder in bridge widening (Wen 2011). Such a bridge widening method has been used in several bridges in Chongqing, China, with a total of 15 spans, and the details of one of these projects are presented in this paper.

For multi-girder bridges, widening leads to redistribution of the internal forces in existing structures; that is, loads on some existing girders may be reduced whereas others may be increased compared with the original design. It is necessary, therefore, to check whether the loading capacity of existing girders is adequate to sustain both dead and live load after widening. Generalised Beam Theory (GBT) is applied to static analyses of steel-concrete composite bridges (Greiner and Camotim 2010), but the results may be indirect. For convenience and efficiency, distribution factors are commonly used for evaluating the live load distribution in multi-girder bridges, and various investigations of the effectiveness of distribution factors have been conducted. In some design codes, these factors are determined using a simple empirical formula (AASHTO Standard Specifications 1996, AASHTO Load and Resistance Factor Design (LRFD) Specifications 2007), and in some cases more complex analytical models have been developed (Li and Shi 1990, Chen *et al*. 2012). As composite girders have much higher flexural and torsional stiffness than concrete girders, use of distribution factors for bridges with only concrete or composite girders may result in either conservative or exaggerated estimates of the live load effect in existing or new girders.

Most previous studies of live load distribution factors have focused on bridge girders with identical cross-sections, and therefore the development of a more precise method for the lateral distribution of live load is essential in evaluating the potential loading capacities of widened bridge systems. In this study, a method for estimating live load distribution factors of a widened bridge with different types of girders was developed, which can also be used for newly built bridges with various girder stiffness or spacing. In the analytical model, the effects of span length, spacing, diaphragms, concrete decks were considered, as well as the torsional and flexural stiffness of both composite box girders and concrete T girders. Finite element analysis of the widened bridge is also presented. These numerical methods are more accurate and applicable than existing analytical or empirical methods. The results were verified and substantiated by results obtained from field tests, and were used to check the validity of design equations from the literature (Barr *et al*. 2001). Our comparative study shows that the AASHTO LRFD specification (2007) procedures and the analytical models closely approximate the live load distribution factors determined by field tests and finite element analysis. Finally, a parameter study was conducted to evaluate the potential load carrying capacities of the existing concrete girders after widening.

2. Project background

The existing Niuerhe Bridge in Chongqing was an 11-span simply-supported highway bridge

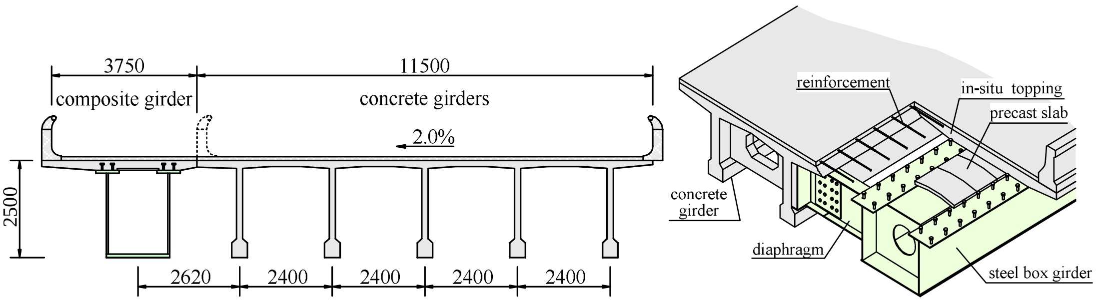

(a) Cross-section view at mid-span (b) Overall view

Fig. 1 Bridge widening project in Chongqing

with 3 lanes. In each span, the bridge had 5 prestressed concrete girders 40 m in length, 2.5 m in height, and with spacing of 2.4 m. As a new overpass was built near the Niuerhe Bridge, widening the existing bridge was the only way to resolve the escalating traffic congestion problem.

Several widening alternatives for the bridge superstructure were considered, such as 1) constructing new girders with cast-in-place concrete; 2) erecting prefabricated concrete girders by movable cranes; and 3) developing a method to build new composite girders and connecting them to the existing superstructure. Widening the bridge with cast-in-place concrete girders needed a large amount of formwork and shoring supports for piers that were over 30 m in height, which was infeasible in both economy and construction time. An “over-the-top” erection method using precast prestressing concrete girders was also precluded, due to the insufficient loading capacity of the existing bridge under the weight of new girders and the cranes. After thorough evaluation of technical, aesthetic, and economic aspects, the preferred solution for the superstructure was a widening system with composite steel-concrete girders. This widening alternative also allowed bridge widening work to proceed without interrupting traffic on the existing bridge that was part of the only highway connecting the two nearest cities.

The widened portion of the superstructure system consists of steel girders, concrete slab, transverse diaphragms, and parapets. The cross-section of the widened bridge at mid-span is shown in Fig. 1. The total depth of the superstructure is 2500 mm, equal to that of the existing concrete girders, with a span-to-depth ratio of 16. The self-weight of the steel girder is 37t, which is about 41% of that of the existing concrete girders. Thus two smaller cranes could be used to erect the steel girder, and the total weight including both the cranes and the steel girder was just within the loading capacities of the existing girders.

Partial-depth precast deck panels with a cast-in-place topping were used over the steel box girders between webs. First, precast concrete deck panels about 1.0×0.7 m in size and 80 mm in thickness were installed over the steel girders. Then the in-situ concrete was poured directly on the precast concrete panels. The thickness of the concrete deck varied from 250 mm above the steel top flange to 120 mm at the cantilever end.

To avoid problems in bridge maintenance and potential safety hazards, the new and old concrete decks were attached rigidly. Also, to achieve better interaction between the new and original superstructures, adequate diaphragms connected to the existing concrete girders were necessary. The spacing of the new diaphragms was consistent with the existing diaphragm spacing. To minimize the stress induced by dead load at the interface between new and existing structures, the diaphragms were not connected to the existing girders before the concrete was poured.

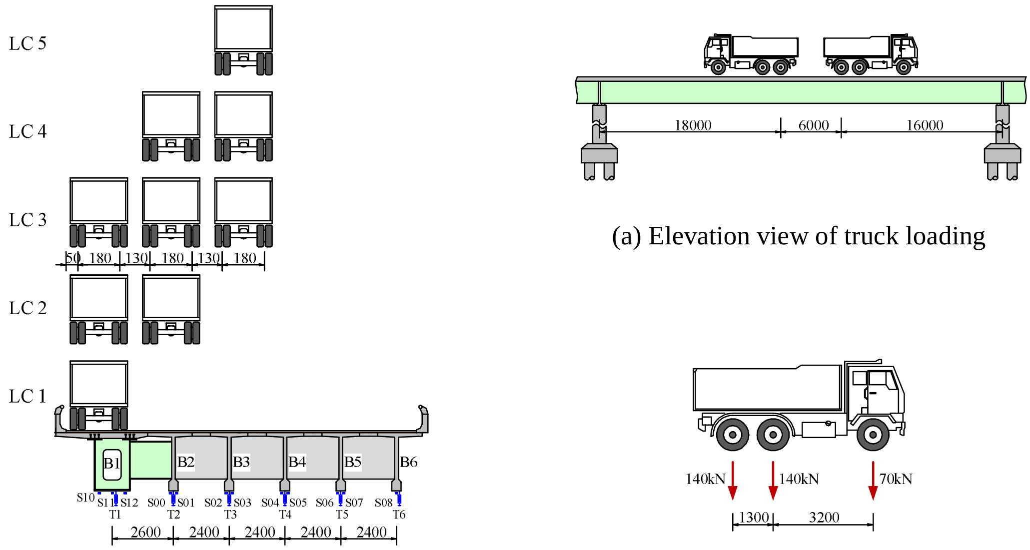

(a) Elevation view of truck loading

(b) Section view of truck loading cases and instrumentation at mid-span

(c) Details of dump truck

Fig. 2 Arrangement of field test

Connections between the widened and existing portions of the structure were properly considered in both design and construction, and it was determined that composite steel-concrete girders would be highly preferable to the alternatives of cast-in-place or prefabricated concrete girders for a number of reasons: reduced traffic disruption with installation of prefabricated steel girders; lower settlement of new piers by virtue of lower weight of superstructure; less long-term deflection due to creep; improved safety both for traffic and construction; minimization of construction time; minimal adverse impacts on the environment.

3. Field test after bridge widening

3.1 Loading conditions

To evaluate the performance of the bridge after widening, a field test was conducted on the first span of the Niuerhe Bridge on the Liangping side. The measured values were also used to calibrate the mathematical models developed in this paper. The girders of the bridge were numbered B1 to B6 from the composite girder to the concrete ones. Six fully loaded three-axle dump trucks with the gross weight of 350±5 kN were used to apply live load to the bridge. The axle load and axle configurations are shown in Fig. 2.

The trucks were placed in various lanes to determine the response of the bridge under live loads. A total of 5 loading cases were conducted in the field test, as shown in Fig. 2(a) and (b). In accordance with the bridge design code of China (JTG D60-2004 2004), the trucks were placed transversely by dividing the bridge into as many 3.1 m wide lanes as possible to generate the most unfavorable actions in the girder. The spacing between the exterior wheels of the trucks and the edge of the parapet was 0.5 m. This arrangement of trucks was much more compact in the

Table 1 Loading efficiency factors of B1

Loading case	LC1	LC2	LC3	LC4	LC5
Loading efficiency factor	0.49	0.83	1.05	0.56	0.21

Table 2 Measured deflections at mid-span (mm)

Girder No.	B1	B2	B3	B4	B5	B6
LC1	6.13	4.57	3.27	1.68	0.38	-0.86
LC2	10.97	8.75	6.50	3.98	1.96	-0.13
LC3	13.82	11.98	9.91	7.05	4.85	2.26
LC4	7.49	7.30	6.66	5.42	4.43	2.89
LC5	2.97	3.14	3.35	3.15	2.87	2.15
Unloading	-0.04	-0.05	-0.02	0.01	0.00	-0.30

Table 3 Measured longitudinal strains of bottom flange at mid-span ($\times 10^{-6}$)

Girder No.	B1	B2	B3	B4	B5	B6
LC1	73	71	43	22	8	-7
LC2	121	117	84	47	22	-2
LC3	148	161	122	83	62	33
LC4	76	95	80	60	57	41
LC5	27	43	41	36	33	38
Unloading	-6	1	0	1	2	2

transverse direction than the width of the lanes. In the longitudinal direction, the trucks were placed near the mid-span of the bridge to generate maximum moment in the simply-supported girders, as shown in Fig. 2(a). For the first three loading cases, truck loadings were performed twice to ensure data reproducibility.

Table 1 lists the loading efficiency factors of composite girder B1 under each loading case, defined as

$$\lambda = \frac{S_{\text{stat}}}{S(1+I_{\text{mp}})} \tag{1}$$

where S_{stat} is the calculated force or displacement under test load, S is the calculated force or displacement under design load, and I_{mp} is the impact factor of vehicles. Since the velocity of trucks in test is relatively slow and the deflection is measured after all trucks are stopped, I_{mp} for test is not considered to simulate the loading condition. The I_{mp} for design is set to 0.45 according to design recommendations based on the bridge design code of China (JTG D60-2004 2004). Strain gauges were placed at the bottom of each concrete girder and steel box girder at the mid-span cross-section. Also, the longitudinal strains of the concrete slab above the steel girder were monitored using strain gauges. To minimize data variation, two or three gauges were placed for each cross-section, and the average measured values were used in the analysis. The instrumentation is presented in Fig. 2(b).

3.2 Test results

The measured deflections and strains at mid-span under each loading cases are presented in Table 2 and Table 3 respectively. The strains listed in Table 3 are the average readings of the two or three gauges on the same girder. It was observed that the bridge exhibited relatively high structural integrity when the trucks loaded on the widened or existing girders. Under loading cases LC1 and LC2, girder B6 deflected upward with compression of the bottom fiber. This is consistent with the well-known reactions of multi-girder bridges under eccentric loading. The maximum measured tension strain was 148×10^{-6} for the composite girder, and 161×10^{-6} for the concrete girders. All responses of the bridge were primarily elastic. Readings from strain gauges and displacement transducers returned nearly zero after each loading, with only slight residual strain or displacement after the tests.

The live load distribution factor can be expressed in the form of maximum displacement or maximum bending moment at mid-span. For the maximum displacement based expression, the load distribution factor is defined as

$$m_i = \frac{\delta_i (EI)_i n_{\mathrm{L}}}{\sum \delta_j (EI)_j} \tag{2}$$

where m_i is the load distribution factor of girder i; δ_i is the mid-span deflection of girder i; n_L is the number of lanes being loaded; $(EI)_i$ is the stiffness of girder i; and j varies from one to the total number of girders. The same notation is used in subsequent equations.

The loading arrangement to generate maximum deflection and moment was the same for simply-supported girders, so the distribution factors for the maximum moment could be formulated in the same manner as that for maximum deflection. Assuming that M_i is the maximum moment for girder i generated by one particular loading condition, the moment-based distribution factors were calculated by the following relationship

$$m_i = \frac{M_i n_{\mathrm{L}}}{\sum M_j} \tag{3}$$

As M_i can be calculated from the simple beam-bending formula by the measured longitudinal strains at the bottom flange, the moment-based distribution factors can also be expressed as

$$m_i = \frac{E_i \varepsilon_i S_i n_{\mathrm{L}}}{\sum E_j \varepsilon_j S_j} \tag{4}$$

where S_i is the sectional modulus of girder i; and ε_i is the longitudinal strains at the bottom of the girder.

In determining the moment inertia of the girders, a transformed-section method was used for composite girders, and the full width of the concrete slab was included for the concrete girders. The concrete modulus of elasticity was derived from the compression strength according to the design code.

The lateral distribution factors derived from the measured displacement or stress at mid-span are presented in Table 4 and Fig. 3. The distribution factors obtained from Eq. (2) and Eq. (4) were nearly equal for each girder. Under the testing loading conditions, the distribution factors were

Table 4 Distribution factors by measured displacement and strain

Girder No.		B1	B2	B3	B4	B5	B6
LC1	Deflection	0.578	0.214	0.153	0.078	0.018	-0.040
	Strain	0.503	0.258	0.157	0.080	0.027	-0.026
LC2	Deflection	1.025	0.405	0.301	0.184	0.091	-0.006
	Strain	0.920	0.471	0.338	0.189	0.089	-0.008
LC3	Deflection	1.289	0.572	0.470	0.333	0.238	0.099
	Strain	1.132	0.652	0.494	0.336	0.251	0.134
LC4	Deflection	0.723	0.349	0.319	0.259	0.212	0.138
	Strain	0.755	0.435	0.330	0.224	0.167	0.089
LC5	Deflection	0.290	0.152	0.162	0.153	0.139	0.104
	Strain	0.301	0.199	0.168	0.126	0.120	0.086

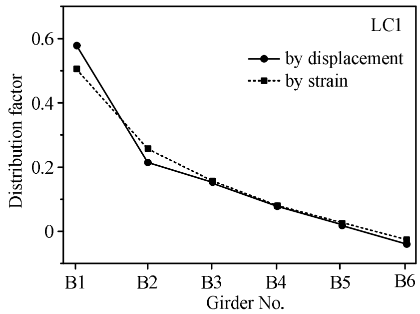

(a) LC1

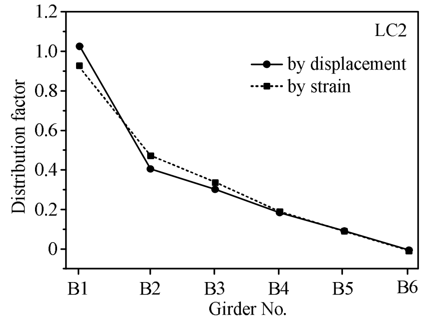

(b) LC2

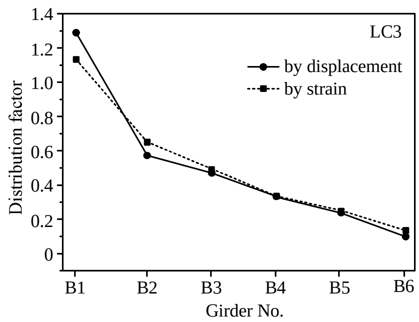

(c) LC3

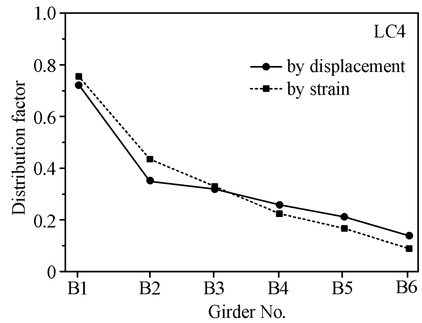

(d) LC4

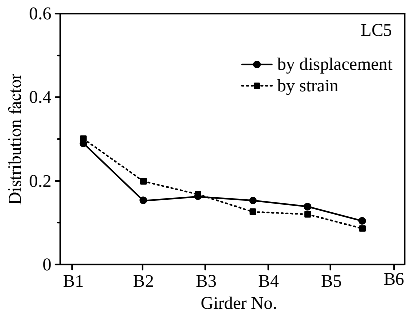

(e) LC5

Fig. 3 Comparison of distribution factors derived between displacement and strain largest in the composite girder (exterior girder) and diminished progressively in the concrete girders. In this way, the load distributed to the existing concrete girders reduced.

4. Calculation of distribution factors

Currently, for convenience and efficiency, distribution factors are often used to estimate the lateral distribution of live load. Since the 1940s, considerable research has been conducted into live load transverse distribution in multi-girder bridges (Newmark *et al*. 1942, Zokaie *et al*. 1991, Suksawang and Nassif 2007). Various analytical and numerical methods have been developed in these investigations, including orthotropic plate theory, grid analysis, finite strip method, finite element method, etc. These studies have also formed the basis of the load lateral distribution factors for bending moments and shear specified in some design codes, such as the AASHTO Standard Specifications (1996) and the AASHTO LRFD (2007). The AASHTO LRFD uses relatively simple expressions for calculating distribution factors, taking into consideration the effects of girder spacing, girder stiffness, span length, skew, and slab stiffness. In China, several analytical models for calculating distribution factors have been developed for different bridge styles and configurations. These models account for more parameters than found in the empirical equations, such as the spacing and stiffness of the diaphragms, and the expressions are also complex in some conditions.

Most of the relevant previous research has been based on I-girder or T-girder bridges, which were different to some extent from box-girder bridges. Normandin and Massicotte (1994) used three-dimensional (3D) finite element methods to study the load lateral distribution of multi-box-girder bridges. Using laboratory tests and finite element analysis, Samaan *et al*. (2005) developed empirical equations for the shear and moment distribution factors for continuous composite bridges with multi-box girders. These methods are applicable to spans ranging from 20 to 100 m and different number of boxes.

For bridge widening, however, girders with different cross-sections or unequal spacing were often used, further complicating the problem of load distribution. Current design codes have not covered this scenario. Chen (1995) used the finite element method for investigating the live load lateral distribution for bridges with unequally spaced girders, subsequently verifying the results by comparison with field test results. As accuracy of distribution factors is important for the design of new girders and the assessment of existing girders in bridge widening projects, analytical methods and finite element models with improved accuracy and applicability were developed in this section, considering the effects of span length, girder pacing, diaphragms, concrete decks, as well as the torsional and flexural stiffness of different type of girders. The applicability of these methods is discussed in later sections.

4.1 Rigid-jointed method

The distribution of live load for multi-girder bridges can be calculated by the rigid-jointed method. The principal assumption of this method is that diaphragm stiffness is relatively very high compared to the stiffness of longitudinal girders. This assumption will be true when a multi-girder bridge has sufficient diaphragms and lower ratios of width to span. According to previous study of concrete *T*-girder bridges (Li and Shi 1990, Yao 2001), the rigid-jointed method is justified when the following relation is satisfied

$$n\sqrt[4]{\beta} \le 1.0, \quad \beta = \frac{\pi^4 I d^3}{3L^4 I_{\mathrm{tr}}} \tag{5}$$

where n is the number of girders; d is half of the slab span between adjacent webs; L is the span of the girder; I is the moment of inertia of the girders; and I_{tr} is the moment of inertia per unit width of concrete slab in the transverse direction.

In this method, the rigid diaphragm distributes the live loads to the main girders in proportion to their relative stiffness. In most conditions, the live load vector may not overlap with the resistance vector of main girders, as torsion of the deck system would occur as a result. To consider this effect, revisions were implemented to take into account the effects of torsional stiffness of the main girders for calculating the distribution factors. The expression of the distribution factor is

$$\eta_{ij} = \frac{(EI)_i}{\sum (EI)_i} + \alpha \frac{(EI)_i a_i}{\sum (EI)_i a_i^2} x_j \tag{6}$$

$$\alpha = \frac{1}{1 + \dfrac{L^2 \Sigma (GI_{\mathrm{t}})_i}{12 \Sigma a_i^2 (EI)_i}} \tag{7}$$

where η_{ij} is the load distribution factor of girder i when the load acts on girder j; α is the correction coefficient derived by considering the torsional stiffness; $(EI)_i$ and $(GI_{\mathrm{t}})_i$ are the flexural stiffness and torsional stiffness of girder i respectively; a_i is the distance between the centroid and the torsion center of girder i; and x_j is the distance from the torsion center of girder i to the loading axis.

The approximate torsional constant I_t for reinforced concrete girders was determined as follows

$$I_{\mathrm{t}} = \sum_{i=1}^{n} a_i b_i t_i^3 \tag{8}$$

$$a_i = \frac{1}{3}\left[1 - 0.63\frac{t_i}{b_i} + 0.052\left(\frac{t_i}{b_i}\right)^5\right] \tag{9}$$

where b_i and t_i are the two sides of each rectangular component of the cross-section with $b_i \ge c_i$; and a_i is the torsion coefficient for the open cross-section.

For a closed cross-section, such as that of composite box girders, the torsional constant I_t is estimated as

$$I_{\mathrm{t}} = \frac{4A^2}{\int_S \frac{ds}{t}} \tag{10}$$

For convenience, the concrete area can be transformed equivalently to the steel section by

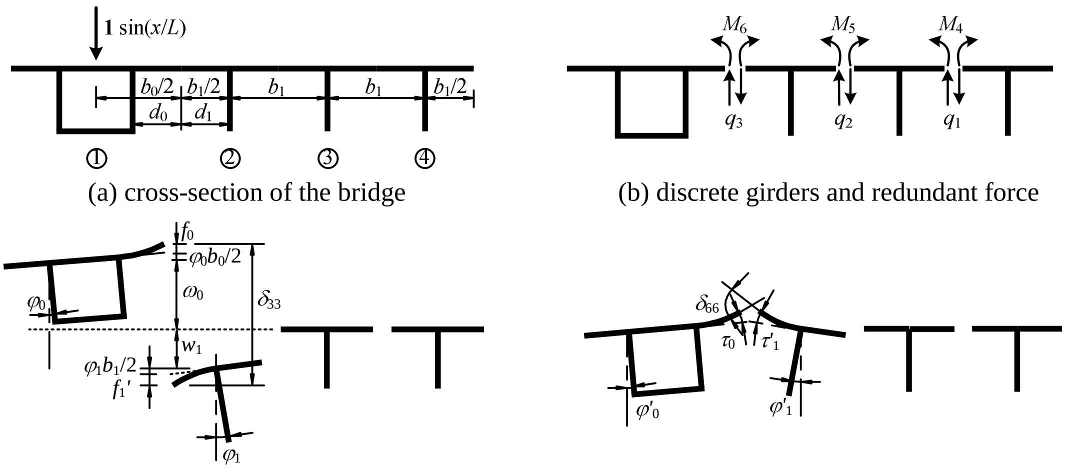

(a) cross-section of the bridge (b) discrete girders and redundant force

(c) solving process of flexibility coefficients

Fig. 4 Analytical model of flexible-jointed method

reducing the slab thickness according to the shear modulus ratio between concrete and steel (Eurocode 4 2005)

$$h_s = h_c G_c / G_s \tag{11}$$

where h_s is the transformed thickness of the concrete slab; h_c is the thickness of the concrete slab; and G_c and G_s are the shear moduli of concrete and steel respectively.

4.2 Flexible-jointed method

In this method, the transverse flexibility of the deck system including the diaphragms and slabs can be considered. The bridge superstructure is divided into a series of discrete girders connected to each other. Using the force method, the redundant force and the moment of the girders can be solved.

For the widened bridge, the superstructures were cut in the longitudinal direction at the center of the slabs, thus freeing the redundant shear and moment, as shown in Fig. 4. The longitudinal shear and normal force at the boundary of each girder element were neglected as their influence was insignificant compared to that of the other forces. To simplify the 3D configuration to a plane one, the moment, shear, and displacement should have the same distribution for each girder. Thus, the unit sinusoidal load was used to simulate the living vehicle load. According to previous study (Li and Shi 1990), the reactions of the girders under this load pattern were consistent for most loading conditions with moving vehicles.

For the widened bridge with different types of girders, the flexural and torsional stiffness ratios are defined as

$$\begin{cases} k_1 = (EI)_0 / (EI)_1 \\ k_2 = (GI_t)_0 / (GI_t)_1 \end{cases} \tag{12}$$

where $(EI)_0$ and $(GI_t)_0$ are the flexural stiffness and torsional stiffness for composite girders respectively; $(EI)_1$ and $(GI_t)_1$ are the flexural stiffness and torsional stiffness for concrete girders respectively.

For continuity of deformations in the bridge, the displacements of each girder at any flange joint must be equal to those of the adjacent girder. The governing equation for this model using the force method can be expressed in matrix form as

$$\left[\delta_{ij}\right]\{q_j\}+\{\Delta_{ip}\}=\mathbf{0} \tag{13}$$

where δ_{ij} is the flexibility coefficient; q_j is the redundant force; and Δ_{ip} is the displacement due to the applied loading.

Taking a widened bridge with three concrete girders and one composite girder as example, the flexibility coefficients are determined as

$$\begin{cases}\delta_{33}=w_0+w_1+f_0+f_1'+\varphi_0\dfrac{b_0}{2}+\varphi_1\dfrac{b_1}{2}=(1/k_1+1+\beta_0+\beta_1'+\gamma((\dfrac{b_0}{b_1})^2/k_2+1))w_1\\ \delta_{36}=\varphi_0-\varphi_1+v_0-v_1'=(\gamma(\dfrac{b_0}{b_1k_2}-1)+1.5\beta_0(\dfrac{b_1}{2d_0})-1.5\beta_1'(\dfrac{b_1}{2d_1}))\dfrac{2w_1}{b_1}\\ \delta_{66}=\dfrac{\varphi_0}{b_0/2}+\dfrac{\varphi_1}{b_1/2}+\tau_0+\tau_1'=(\gamma(1/k_2+1)+3\beta_0(\dfrac{b_1}{2d_0})^2+3\beta_1'(\dfrac{b_1}{2d_1})^2)w_1(\dfrac{2}{b_1})^2\\ \delta_{11}=\delta_{22}=2(w_1+f_1+\varphi_1\dfrac{b_1}{2})=2(1+\beta_1+\gamma)w_1\\ \delta_{44}=\delta_{55}=2(\dfrac{\varphi_1}{b_1/2}+\tau_1)=2(\gamma+3\beta_1(\dfrac{b_1}{2d_1})^2)w_1(\dfrac{2}{b_1})^2\\ \delta_{12}=\delta_{23}=(\dfrac{\varphi_1}{b_1/2}-w_1)=(\gamma-1)w_1\\ \delta_{24}=\delta_{35}=-\delta_{15}=-\delta_{26}=\varphi_1=\gamma w_1\dfrac{2}{b_1}\\ \delta_{45}=\delta_{56}=-\dfrac{\varphi_1}{b_1/2}=-\gamma w_1(\dfrac{2}{b_1})^2\end{cases} \tag{14}$$

where $\beta_0=f_0/w_1$; $\beta_0=f_0/w_1$; $\beta_1=f_1/w_1$; $\beta'_1=f_1'/w_1$; $\gamma=\varphi_1 b_1/2w_1$; $w_0=L^4/\pi^4(EI)_0$ and $w_1=L^4/\pi^4(EI)_1$ are the deflections at mid-span under unit sinusoidal load for the composite and concrete girders respectively; $\varphi_0=b_0L^2/2\pi^2(GI_t)_0$ and $\varphi_1=b_1L^2/2\pi^2(GI_t)_1$ are the torsion angles at mid-span under unit sinusoidal load for the composite and concrete girders respectively; $f_0=d_0^3/3(EI)_{tr0}$ and $f_1=d_1^3(EI)_{tr1}$ are the deflections of the cantilever end under unit shear for the composite and concrete girders respectively; $v_0=d_0^2/2(EI)_{\mathrm{tr}0}$ and $v_1=d_1^2/2(EI)_{\mathrm{tr}1}$ are the rotations of the cantilever end under unit shear for the composite and concrete girders respectively; $\tau_0=d_0/(EI)_{\mathrm{tr}0}$ and $\tau_1=d_1/(EI)_{\mathrm{tr}1}$ are the rotations of the cantilever end under unit moment for the composite and concrete girders respectively; $(EI)tr0$ and $(EI)tr1$ are the stiffness of the diaphragms, shown in Fig. 5.

The symbols in the above formulas are also explained in Fig. 4. To represent the unequal transverse stiffness of slab and diaphragm, a prime was added to the displacement variable between the composite and concrete girders, and is shown in Fig. 4(c).

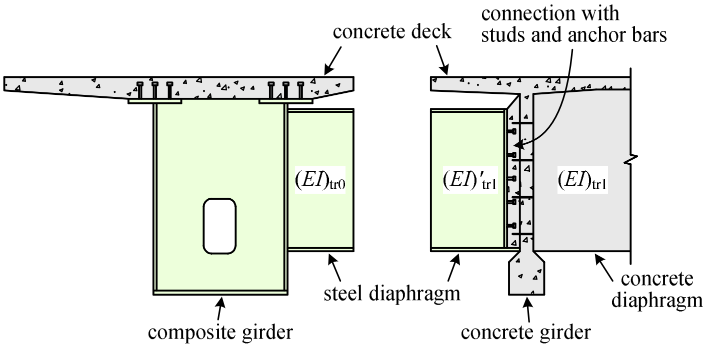

Fig. 5 Diaphragm between composite and concrete girders

Substituting the flexibility coefficients from Eq. (14) into Eq. (13), the governing flexibility equation for the widened bridge with three concrete girders and one composite girder can be formulated as

$$\begin{bmatrix} \delta_g & \gamma-1 & 0 & 0 & -\gamma & 0 \\ \gamma-1 & \delta_g & \gamma-1 & \gamma & 0 & -\gamma \\ 0 & \gamma-1 & \delta_{33} & 0 & \gamma & \delta_{36} \\ 0 & \gamma & 0 & \delta_x & -\gamma & 0 \\ -\gamma & 0 & \gamma & -\gamma & \delta_x & -\gamma \\ 0 & -\gamma & \delta_{63} & 0 & -\gamma & \delta_{66} \end{bmatrix} \begin{Bmatrix} q_1 \\ q_2 \\ q_3 \\ M_4/0.5b_1 \\ M_5/0.5b_1 \\ M_6/0.5b_1 \end{Bmatrix} = \begin{Bmatrix} 0 \\ 0 \\ 1/k_1 \\ 0 \\ 0 \\ 0 \end{Bmatrix} \tag{15}$$

where $\delta_g = 2 + 2\gamma + 2\beta_1$; and $\delta_x = 2\gamma + 6(b_1/2d_1)^2\beta_1$.

Solving Eq. (15) for the unknown force q_j and using the equilibrium condition, the load sustained by each girder could be determined.

For the diaphragm between the composite girder and the exterior concrete girder shown in Fig. 5, the stiffness was composed of two parts: the transverse steel girders and the concrete decks above. Because of the large span-to-depth ratio of the diaphragm, the stiffness was calculated by considering the shear deformation using the formula

$$(EI)_{eq} = \frac{EI}{1 + \dfrac{3\mu EI}{GA_d L_d^2}} \tag{16}$$

where A_d and L_d are the area and span of steel diaphragm respectively; and μ is the shape factor accounting for the distribution of shear stresses across the section. For I girders, μ equals the ratio of cross-section area to the web area.

4.3 Finite element analysis

The finite element program MSC Marc was used to perform the analytical study of the widened bridge. The objective was to examine the response of the widened bridge, which was difficult to

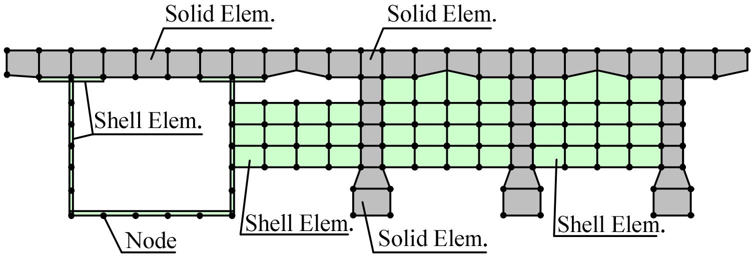

Fig. 6 Finite element model using solid and shell elements (FEM-SS)

measure during tests. The finite element models were also used to validate the analytical models proposed in this paper by parametric study.

Two types of detailed 3D finite element models were established for the widened bridge. Model FEM-SS used solid and shell elements to represent the concrete slab and steel girders, with the advantages of avoiding rigid link elements and modeling the bridge with more detail; model FEM-BS used beam elements to represent the steel and concrete girders, with the advantages of fewer elements and higher efficiency in computation.

In the FEM-SS model, the concrete slabs were represented by 8-node solid elements and the steel girders and diaphragms were modeled by 4-node shell elements. The modulus of elasticity was assumed to be 2.06×10^5 MPa for steel and 3.25×10^4 MPa for concrete; the Poisson's ratio was assumed to be 0.3 for steel and 0.2 for concrete. Full composite interaction between the steel girders and the concrete slab was assumed in the model.

The girders rested on 400×350×57 mm rubber bearings. The bearings were modeled by restricting vertical translations for the bottom flange nodes at the end of each girder, and spring elements were also used to model the lateral constraint, with the horizontal stiffness defined as

$$K_{\mathrm{b}} = \frac{G_{\mathrm{b}} A_{\mathrm{b}}}{\sum t_{\mathrm{b}}} \tag{17}$$

where K_b is the horizontal stiffness of the bearings; G_b is the dynamic shear modulus of the bearings; A_b is the shear area of the bearing; and $\sum t_{\mathrm{b}}$ is the total thickness of the rubber layers.

The locations of the load were consistent with the dump trucks in the field tests. Wheels were considered as point loads acting on the top surface of the concrete deck. If the wheel placement was not on an element node, the vertical force was interpolated between the nearest four nodes with the equivalence of the whole wheel load. The FE model built with solid-shell elements is shown in Fig. 6.

The modeling approach using both beam and shell elements had been verified by previous work on concrete girder bridges (Barr *et al*. 2001). Both the longitudinal girders and the diaphragms were modeled using 3D two-node beam elements, and the concrete slab was modeled using 4-node shell elements. The girders were made to act in conjunction with the concrete slabs by connecting the centroid of the beam elements (longitudinal girders and diaphragms) and shell elements (concrete slab) with rigid link elements. The rigid link elements are modeled to represent the presence of transverse connection beam. Since the transverse connection beam are closely located in the structure, the effect of transverse connection is pretty high and this effect has to be considered as rigid link elements by setting the interior deformation within this region to zero. The

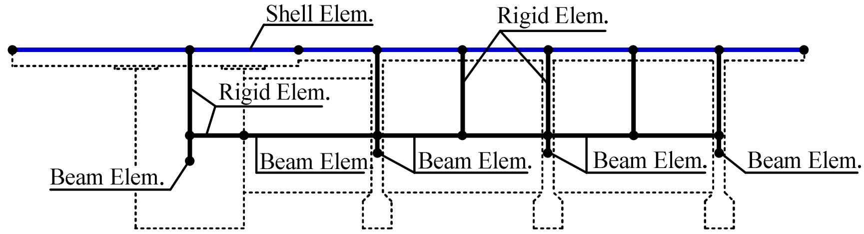

Fig. 7 Finite element model using beam and shell elements (FEM-BS)

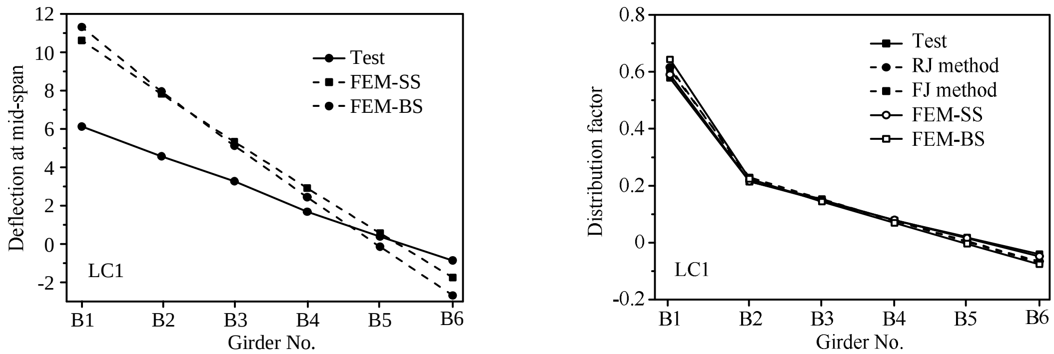

(a) Deflections (b) Moment distribution factors at mid-span

Fig. 8 Comparison between field test and calculation for loading case LC1

finite element model of FEM-BS is illustrated in Fig. 7. The same material properties and boundary conditions were used for FEM-BS as for FEM-SS.

The element dimensions of FEM-SS and FEM-BS were nearly identical, with the node spacing being about 400 mm for concrete slabs and girders. FEM-SS had approximately 11000 elements and 18500 nodes; and FEM-BS had approximately 3800 elements and 3400 nodes.

4.4 Comparison of calculated results and test results

Fig. 8(a) shows the comparison between the calculated and measured deflections at mid-span for loading case LC1. The calculated deflections of FEM-SS are close to those of FEM-BS, but the calculated deflections are greater than the measured deflections for most girders. The comparisons for loading cases LC2 to LC5 had similar results. Under each loading case, an almost linear distribution of deflection occurred at the cross-section, showing good integrity of the widened superstructure.

Fig. 8(b) and Table 5 show the comparison between the experimental and analytical results for the load distribution factors. Reasonable agreement can be observed between the results obtained by field tests, theoretical model, and finite element analysis. On the basis of this verification, the same finite element modeling method was applied to analyze the bridges through a parametric study.

There are two main reasons for the gap between FEM models and tests. The first reason is underestimating of young’s modulus of concrete. In nonlinear analysis, it is widely accepted to employ the parabolic equation for the stress-strain relationship as following

Table 5 Comparison of distribution factors from field tests and theoretical analysis

Girder No.		B1	B2	B3	B4	B5	B6
LC1	Test	0.578	0.214	0.153	0.078	0.018	-0.040
	RJ method*	0.616	0.220	0.148	0.077	0.005	-0.066
	FJ method	0.608	0.229	0.153	0.077	0.003	-0.070
	FEM-SS	0.590	0.216	0.147	0.080	0.016	-0.048
	FEM-BS	0.643	0.224	0.144	0.069	-0.004	-0.076
LC2	Test	1.025	0.405	0.301	0.184	0.091	-0.006
	RJ method	1.050	0.397	0.294	0.190	0.087	-0.017
	FJ method	1.066	0.434	0.311	0.186	0.063	-0.060
	FEM-SS	1.024	0.401	0.297	0.194	0.092	-0.008
	FEM-BS	1.090	0.409	0.292	0.179	0.069	-0.040
LC3	Test	1.289	0.572	0.470	0.333	0.238	0.099
	RJ method	1.319	0.535	0.436	0.336	0.237	0.137
	FJ method	1.340	0.579	0.460	0.335	0.207	0.080
	FEM-SS	1.292	0.543	0.445	0.343	0.239	0.138
	FEM-BS	1.349	0.548	0.440	0.329	0.222	0.112
LC4	Test	0.723	0.349	0.319	0.259	0.212	0.138
	RJ method	0.704	0.315	0.287	0.259	0.231	0.203
	FJ method	0.732	0.350	0.307	0.257	0.204	0.149
	FEM-SS	0.701	0.327	0.298	0.263	0.224	0.187
	FEM-BS	0.705	0.324	0.295	0.261	0.225	0.190
LC5	Test	0.290	0.152	0.162	0.153	0.139	0.104
	RJ method	0.264	0.137	0.142	0.147	0.152	0.157
	FJ method	0.273	0.146	0.149	0.148	0.144	0.139
	FEM-SS	0.268	0.142	0.148	0.149	0.148	0.146
	FEM-BS	0.258	0.139	0.147	0.151	0.152	0.153

*RJ method: rigid-joint method; FJ method: flexible-joint method

$$\sigma = \sigma_0[2(\frac{\varepsilon}{\varepsilon_0}) - (\frac{\varepsilon}{\varepsilon_0})^2] \quad \varepsilon \le \varepsilon_0 \tag{18}$$

where σ is the stress of concrete; ε is the strain of concrete; σ_0 is the peak stress of concrete; ε_0 is the peak strain of concrete which is normally set as 0.002. By differentiating the stress-strain relationship, the elastic modulus of concrete can be set as

$$E_c = \frac{2\sigma_0}{\varepsilon_0} = 2 \times \frac{40\text{MPa}}{0.002} = 40\text{GPa} \tag{19}$$

Hence, the elastic modulus of concrete defined by Eq. (18) is 40 Gpa for concrete and is 23% higher than the value employed by FEM models. This deviation can explain the overestimation of deflection of FEM models.

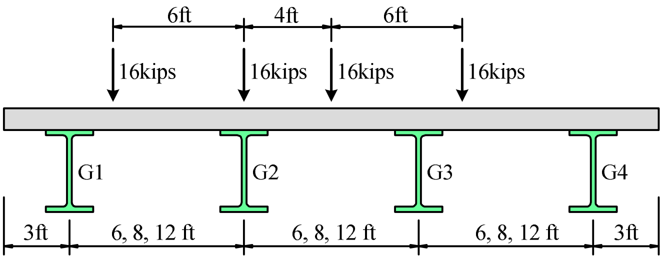

Fig. 9 Bridge cross-section and position of HS20 trucks

Table 6 Comparison of distribution factors for girder G2

L (ft)	*S* (ft)	AASHTO (1996)	AASHTO (1998)	Tarhini (1995)	Bakht (1988)	RJ method	FJ method	FEM	$n_1\sqrt[4]{\beta_1}$
35	6	1.09	1.24	1.19	0.93	1.01	1.04	1.05	3.00
	8	1.45	1.52	1.46	1.24	1.10	1.49	1.56	3.15
	12	2.18	2.05	1.85	1.86	1.33	2.05	2.26	3.32
45.5	6	1.09	1.16	1.08	0.88	1.01	1.02	1.05	2.31
	8	1.45	1.42	1.35	1.18	1.09	1.37	1.47	2.42
	12	2.18	1.90	1.74	1.77	1.33	1.84	2.09	2.56
56	6	1.09	1.10	0.99	0.86	1.00	0.99	1.01	1.88
	8	1.45	1.34	1.27	1.14	1.09	1.27	1.35	1.97
	12	2.18	1.80	1.66	1.72	1.33	1.67	1.86	2.08
77	6	1.09	1.01	0.92	0.83	0.99	0.94	0.96	1.37
	8	1.45	1.26	1.19	1.10	1.08	1.16	1.23	1.43
	12	2.18	1.65	1.58	1.66	1.33	1.47	1.62	1.51
98	6	1.09	0.95	0.95	0.81	0.97	0.91	0.93	1.07
	8	1.45	1.16	1.23	1.08	1.07	1.10	1.16	1.12
	12	2.18	1.54	1.62	1.62	1.33	1.40	1.51	1.19
119	6	1.09	0.90	1.10	0.80	0.95	0.89	0.91	0.88
	8	1.45	1.10	1.38	1.07	1.07	1.08	1.13	0.93
	12	2.18	1.46	1.77	1.60	1.33	1.36	1.46	0.98
Average and standard deviation of errors for predictions compared with FEM results									
Average		1.16	1.01	1.01	0.90	0.87	0.94	1.00	-
STDEV		0.16	0.07	0.12	0.09	0.14	0.03	0.00	-

The second reason is the existence of ribbed stiffener inside the retrofit steel girder which was not considered in FEM modelling. In actual bridges, the stiffener would enhance the steel girder by eliminating the deformation of the web of the beam. However, this was not considered in FEM models.

4.5 Discussion of analytic and modeling results

The methods developed above and those from several design codes were evaluated by

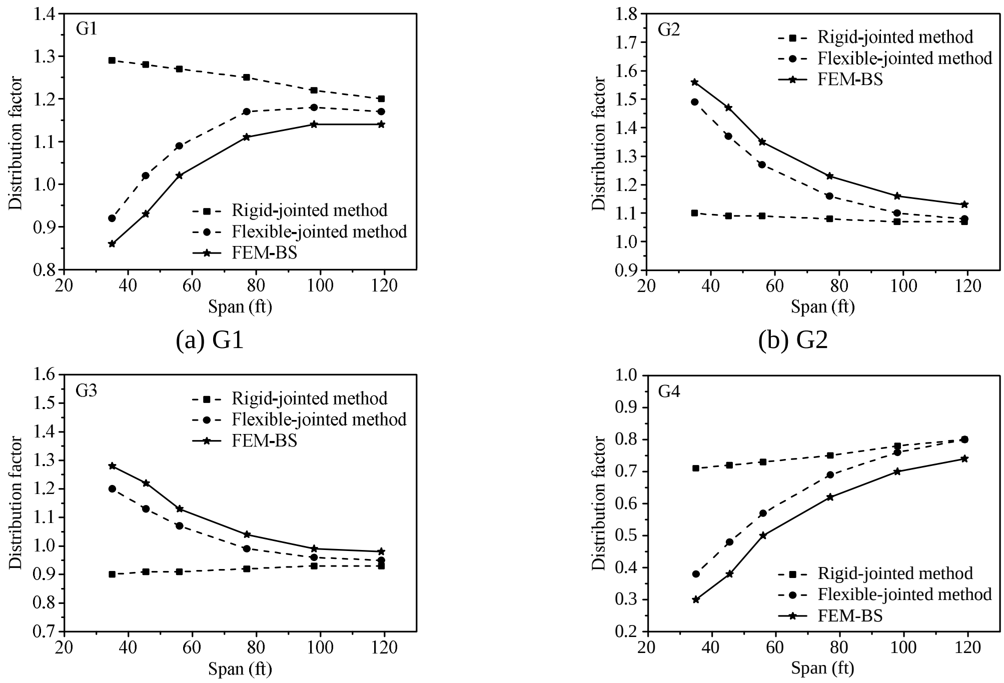

(a) G1 (b) G2

(c) G3 (d) G4

Fig. 10 Variation in distribution factors with bridge span

application to bridge examples from Mabsout *et al*. (1997). The geometry and cross-section dimensions of the selected bridges are represented in Fig. 9. The spans of the selected bridges were 35 ft (10.67 m), 45.5 ft (13.87 m), 56 ft (17.07 m), 77 ft (23.47 m), 98 ft (29.87 m), and 119 ft (36.27 m). The concrete deck was 7.5 in (190 mm) thick, and was supported by four W36×160 steel girders. The spacing of the girders was 6 ft (1.83 m), 8 ft (2.44 m), and 12 ft (3.66 m). AASHTO design trucks (HS20) were positioned on the bridge to produce the maximum moment in the mid-span, as also shown in Fig. 9. The bridges had at least two lanes, and they were loaded by placing HS20 trucks on all lanes.

To evaluate the various methods for calculating live load distribution factors, calculated results from finite element analysis were compared with the AASHTO LRFD Specifications (2007), AASHTO Standard Specifications (1996), research results of Bakht and Mose (1988), Tarhini and Frederick (1995), the rigid-jointed method, and the flexible-jointed method proposed in this paper. Distribution factors for wheel load of girder G2 predicted by the various methods are presented in Table 6, including those predicted by finite element method. $n_1\sqrt[4]{\beta_1}$ is the discriminant for the application range of the rigid-jointed method defined in Eq. (5). The distribution factors listed in the table are expressed in terms of wheel load, so they should be multiplied by 0.5 to compare with the distribution factors for axle load defined in the design codes.

As its adaptability is not limited by the width and length of the bridge, the finite element method was used to validate the results obtained by other methods. The following observations can be drawn from Table 6: 1) The empirical equations for moment distribution factors in AASHTO specification (1996) mainly consider the spacing of the longitudinal girders, which agrees well

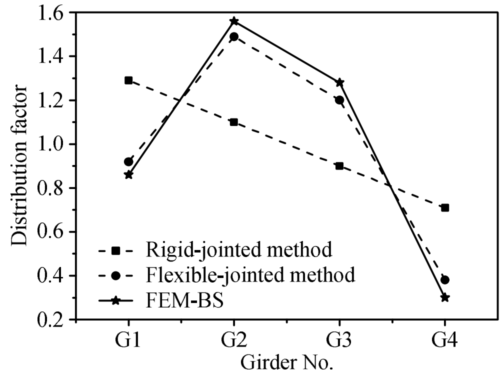

Fig. 11 Comparison of live load distribution factors for bridge with 35 ft span and 30 ft in width

Table 7 Comparison of distribution factors before and after widening for Niuerhe Bridge

Girder No.		B1	B2	B3	B4	B5	B6
Niuerhe Bridge (L=40m)	(1) Before widening	-	0.817	0.607	0.466	0.607	0.817
	(2) After widening	1.055	0.423	0.385	0.433	0.515	0.633
	(2) / (1)	-	0.518	0.634	0.929	0.848	0.775

Table 8 Multiple presence factors (JTG D60-2004 2004)

Number of lanes	1	2	3	4	5	6	7
Multiple presence factors	1.0	1.0	0.78	0.67	0.55	0.52	0.50

with the finite element method for short span bridges, but produces conservative results for long spans. 2) Good agreement is shown between the results from the AASHTO LRFD specification (2007) and the finite element method. 3) The equations proposed by Bakht and Mose (1988) and Tarhini and Frederick (1995) consider girder spacing and span simultaneously, and the predictions have relatively large discrepancies from the finite element results in some cases. 4) The rigid-jointed method also shows large discrepancies and it cannot take into account variation of girder spacing and span. 5) The flexible-jointed method predicts load distribution factors similar to those by the finite element method, but all the values for interior girders are underestimated by 7% at most.

Fig. 10 shows the effect of span length on the moment distribution factors for interior and exterior girders due to truck load arranged as shown in Fig. 9. In the figure, all bridges have the same width. Predictions based on the flexible-jointed method compare well with the finite element results, but give higher predictions (by about 10%) for exterior girders and smaller predictions (by about 8%) for interior girders. As the width for these bridges was kept constant, their span variation also represented the variation in the span-to-width aspect ratio of the superstructures, which ranged from 0.86 to 0.25 for the analyzed bridges. According to the finite element results, for longer span lengths or smaller aspect ratios, the moment distribution factor increased for the exterior girder and decreased for the interior girder. This also means that better moment distribution between girders was achieved when the span length increased or the aspect ratio decreased.

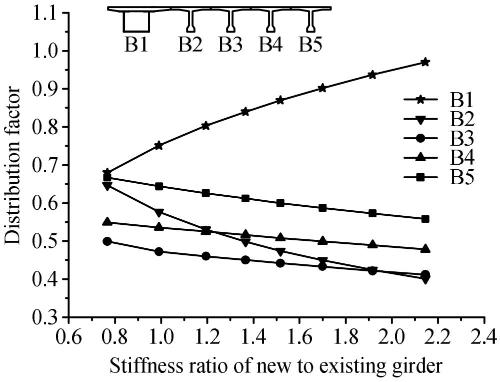

(a) for bridge with 4 concrete girders

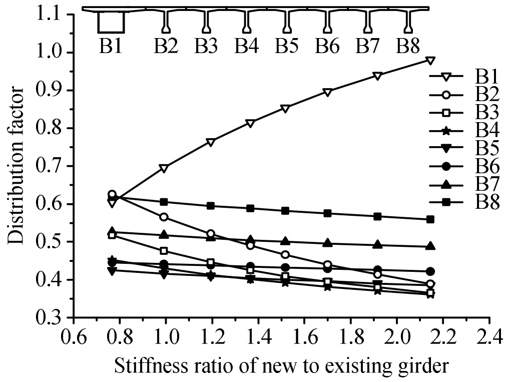

(b) for bridge with 7 concrete girders

Fig. 12 Effect of new girder stiffness on distribution factors (widened by one side)

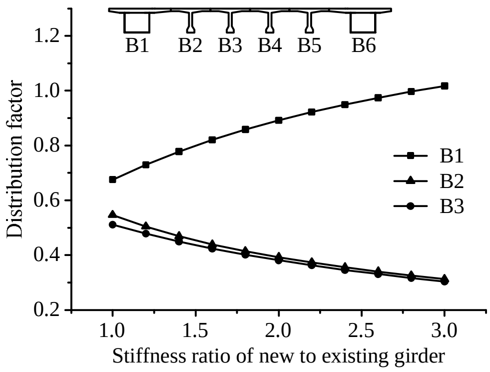

(a) for bridge with 4 concrete girders

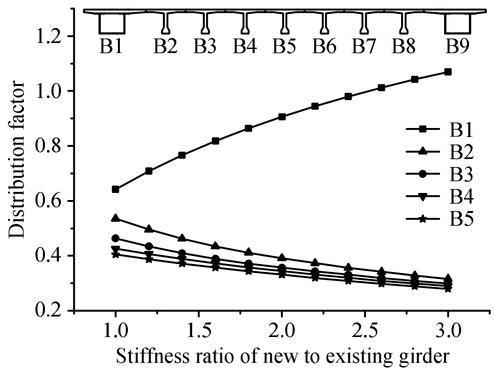

(b) for bridge with 7 concrete girders

Fig. 13 Effect of new girder stiffness on distribution factors (widened by both sides)

For a bridge with the span of 35 ft and width of 30 ft, the distribution factors for each girder are shown in Fig. 11. The predictions by the flexible-jointed method are close to the finite element values for each girder, with an overestimation by about 20% at most because of the small distribution factor of G4 for exterior girders. This also implies that the rigid-jointed method would yield inaccurate results for bridges with a wide deck.

5. Analysis of load capacity of existing girders after widening

Live load distribution factors are used to obtain the moment or shear for each girder in bridge design. For a particular girder, a higher distribution factor suggests a higher sustained load. As the composite box girder has much higher stiffness, the distribution factors of the concrete *T* girders will decrease after widening. This means an increase in potential loading capacity for the overall structure.

The live load distribution factors calculated using finite elements analysis for Niuerhe Bridge before and after widening are shown in Table 7. Multiple presence factors (JTG D60-2004 2004) presented in Table 8 were applied to account for multiple-lane loading. Table 7 shows that the distribution factors for the existing girders diminished after widening, with the maximum 40.4% drop for the concrete girder adjacent to the composite box girder. The distribution factor of the exterior concrete girder B6 opposite the widened side also decreased, but the value was still 49.6% larger than that of girder B2. As the Niuerhe Bridge had uniform design loading capacities for all interior and exterior girders, the potential load capacity of concrete girders for carrying living load would increase about 17.4%. This also would be the case even if the decrease caused by multiple presence factors were not considered.

To investigate the loading capacity of the existing girders after widening, the effect of the new girder stiffness on the distribution factors was evaluated using the finite element method. Fig. 12 and Fig. 13 show the distribution factors with different stiffness or quantities of girders for bridges with a span of 40 m. The distribution factors shown in the figures are the maximum values generated by the most unfavorable loading positions for each girder, and the effect of multiple presence factors presented in Table 8 was also included.

It is observed that the moment distribution factor decreases with the increase of the new girder stiffness. For a certain number of girders, the distribution factors for a bridge widened on both sides are much lower than for a bridge widened on single side. It should be noted that the distribution factors for all concrete girders are very similar for the double-side-widened bridge with high stiffness new girders. In practice, therefore, it is unnecessary to design new girders with very high stiffness, as this will introduce higher stresses or forces at the interface between new and existing slabs or diaphragms, leading to problems in maintenance and durability.

6. Conclusions

This paper presented a multi-girder bridge widened with composite steel and concrete box girders. As the performance of the widened bridge was greatly affected by the lateral distribution of live loads, extensive theoretical and experimental investigations were conducted to determine the distribution factors on bridge girders with uneven stiffness. The actual practice of the Niuerhe Bridge and our theoretical research can provide valuable information for superstructure design in bridge widening projects or in new bridges with unequal girders. From the results of our tests and analyses, the following conclusions can be drawn

- The widening of Niuerhe Bridge using composite steel-concrete girders resulted in a satisfactory solution in both technical and economic aspects. These include improving the loading capacity of existing girders, avoiding traffic disruption during construction, incorporating a lighter weight for erection, thus leading to faster construction and better mechanical performance.
- Analytical formulations were deduced for calculating the moment distribution factors for bridges with different girder types of. The proposed methods considered factors of diaphragm, concrete decks, span length, and girder spacing, as well as the torsional and flexural stiffness of the both composite box girders and concrete T girders. Good agreement between the results from analytic formulation and those from finite element analysis and field tests demonstrated the accuracy and effectiveness of the analytic formulation.
- Two detailed finite element models of the widened bridge, using solid-shell elements or beam-shell elements, were developed, and accurately reproduced the displacements and moments according to comparison with the measurements from field tests.

- The distribution factors decreased with an increase in the stiffness of the new girders. This decrease would improve the potential loading capacity for the existing girders to carry live load. Moreover, a bridge widened on both sides would be more effective in decreasing the distribution factors for intermediate girders than that widened on a single side.

Acknowledgement

This research was supported by the National Natural Science Foundation of China (51138007). The assistance of Yudong Branch of Chongqing Expressway Development Co., Ltd. in the field test is greatly appreciated.

References

ASTM C 469 (2002), *Standard test method for static modulus of elasticity and Poission's ratio Concrete in Compression,* Annual Book of ASTM Standards, Pennsylvania, USA.

Berndt, M.L. (2009), "Properties of sustainable concrete containing fly ash, slag and recycled concrete aggregate", *Constr. Build. Mater.*, **23**(9), 2609-2613.

Berra, M., Carassiti, F., Mangialardi, T., Paolini, A.E. and Sebastiani, M. (2012), "Effects of nanosilica addition on workability and compressive strength of Portland cement pastes", *Constr. Build. Mater.*, **35**, 666-675.

Chang, C.Y., Huang, R., Lee, P.C. and Weng, T.L. (2011), "Application of a weighted Grey Taguchi method for optimizing recycled aggregate concrete mixture", *Cem. Concr. Comp.*, **33**(10), 1038-1049.

Coelho, A. and de Brito, J. (2011), "Distribution of materials in construction and demolition waste in Portugal", *Waste Manage Res.*, **29**(8), 843-853.

De Juan, M.S. and Gutiérrez, P.A. (2009), "Study on the influence of attached mortar content on the properties of recycled concrete aggregate", *Constr. Build. Mater.*, **23**(2), 872-877.

Del Río Merino, M., Gracia, P.I. and Azevedo, I.S.W. (2010), "Sustainable construction: construction and demolition waste reconsidered", *Waste Manage Res.*, **28**(2), 118-129.

Elhakam, A.A., Mohamed, A.E. and Awad, E. (2012), "Influence of self-healing, mixing method and adding silica fume on mechanical properties of recycled aggregates concrete", *Constr. Build. Mater.*, **35**, 421-27.

Hao, J.L., Hills, M.J. and Tam, V.W. (2008), "The effectiveness of Hong Kong's construction waste disposal charging scheme", *Waste Mange Res.*, **26**(6), 553-558.

Hosseini, P., Booshehrian A. and Madari, A. (2011), Developing concrete recycling strategies by utilization of nano-SiO2 Particles, *Waste Biomass Valor.*, **2**(3), 347-355.

IS 1331 (1992), *Indian Standard Non-Destructive Testing of Concrete-Method of Test: Part 1 Ultrasonic Pulse Velocity*, Bureau of Indian Standards, New Delhi, India.

IS 1331 (1992), *Indian Standard Non-Destructive Testing of Concrete-Method of Test: Part 2 Rebound Hammer*, Bureau of Indian Standards, New Delhi, India.

IS 2386 (1963), *Methods of Test for Aggregates for Concrete*, Bureau of Indian standards, New Delhi, India.

IS 383 (1970), *Specification for Coarse and Fine Aggregates*, Bureau of Indian standards, New Delhi, India.

IS 5816 (1999), *Indian Standard Splitting Tensile Strength of Concrete-Method of Test*, Bureau of Indian Standards, New Delhi, India.

Limbachiya, M., Meddah, M.S. and Ouchagour, Y. (2012), "Use of recycled concrete aggregate in fly-ash concrete", *Constr. Build. Mater.*, **27**(1), 439-449.

Lin, K.L., Wu, H.H., Shie, J.L., Hwang, C.L. and Cheng, A. (2010), "Recycling waste brick from construction and demolition of buildings as pozzolanic materials", *Waste Manage Res.*, **28**(7), 653-659.

Lin, Y.H., Tyan, Y.Y., Chang, T.P. and Chang, C.Y. (2004), "An assessment of optimal mixture for concrete

made with recycled concrete aggregates”, *Cem. Concr. Res.*, **34**(8), 1373-1380.
Minitab v16 (2010), Minitab Inc.
Montgomery, D.C. (2012), *Design and Analysis of Experiment*, John Wiley and Sons Inc., New York, USA.
Mukharjee, B.B. and Barai, S.V. (2014), “Influence of nano-silica on the properties of recycled aggregate concrete”, *Constr. Build. Mater.*, **55**, 29-37.
Neville, A.M. (2012), *Properties of Concrete*, Pearson Education India, New Delhi, India.
Olivia, M. and Nikraz, H. (2012), “Properties of fly ash geopolymer concrete designed by Taguchi method”, *Mater. Des.*, **36**, 191-198.
Ozbay, E., Oztas, A., Baykasoglu, A. and Ozbebek, H. (2009), “Investigating mix proportions of high strength self compacting concrete by using Taguchi method”, *Constr. Build. Mater.*, **23**(2), 694-702.
Pacheco-Torgal, F., Miraldo, S., Ding, Y. and Labrincha, J.A. (2013), “Targeting HPC with the help of nanoparticles: An overview”, *Constr. Build. Mater.*, **38**, 365-370.
Poon, C.S., Kou, S.C. and Lam, L. (2002), “Use of recycled aggregates in molded concrete bricks and blocks”, *Constr. Build. Mater.*, **16**(5), 281-289.
Qing, Y., Zenan, Z., Deyu, K. and Rongshen, C. (2007), “Influence of nano-silica addition on properties of hardened cement paste as compared with silica fume”, *Constr. Build. Mater.*, **21**(3), 539-545.
Rakshvir, M. and Barai, S.V. (2006), “Studies on recycled aggregates-based concrete”, *Waste Manage Res.*, **24**(3), 225-233.
Rao, M., Bhattacharya, S.K. and Barai, S.V. (2009), “Influence of field recycled coarse aggregate on properties of concrete”, *Mater. Struct.*, **44**(1), 1163-1167.
Roy, R.K. (2001), *Design of Experiments Using the TAGUCHI Approach: 16 Steps to Product and Process*, John wiley and sons Inc., New York, USA.
Said, A.M., Zeidan, M.S., Bassuoni, M.T. and Tian, Y. (2012), “Properties of concrete incorporating nano-silica”, *Constr. Build. Mater.*, **36**, 838-844.
Tam, V.W. and Tam, C.M. (2009), “Parameters for assessing recycled aggregate and their correlation”, *Waste Manage Res.*, **27**(1), 52-58.
Tam, V.W., Kotrayothar, D. and Loo, Y.C. (2009), “On the prevailing construction waste recycling practices: a South East Queensland study”, *Waste Manage Res.*, **27**(2), 167-174.
Turkmen, I., Gul, R. and Celik, C. (2008), “A Taguchi approach for investigation of some physical properties of concrete produced from mineral admixtures”, *Build. Envir.*, **43**(6), 1127-1137.

CC